

Supporting Information

A carbonyl-rich covalent organic framework as high-performance cathode material for aqueous rechargeable zinc-ion battery

Dingxuan Ma,^a Huimin Zhao,^a Fan Cao,^c Huihui Zhao,^a Jixin Li,^d Lei Wang,^{*,b} and Kang Liu^{*,a}

^a College of Chemistry and Molecular Engineering, Key Laboratory of Optic-Electric Sensing and Analytical Chemistry for Life Science, MOE, Shandong Key Laboratory of Biochemical Analysis, Qingdao University of Science and Technology, Qingdao 266042, P. R. China.

^b College of Environment and Safety Engineering, Qingdao University of Science and Technology, Qingdao 266042, P. R. China.

^c School of Materials Science and Engineering, Shandong Jianzhu University, Jinan 250101, Shandong, P. R. China.

^d State Key Laboratory of Inorganic Synthesis and Preparative Chemistry, College of Chemistry, Jilin University, Changchun 130012, P. R. China.

Contents:

- General information
- Synthetic Procedures
- Characterization
- Structure simulations and powder X-ray diffraction analyses
- Electrochemical measurement
- Theoretical calculation
- References

General information

All starting chemicals and solvents were obtained from TCI or Sigma Aldrich, and used without further purification. ^1H NMR spectra were recorded on a Bruker AVAN CE NEO 400. Fourier transform infrared (FT-IR) spectra were recorded on the Nicolet Impact 410 FT-IR spectrometer. Solid-state ^{13}C CP/MAS NMR was performed on Agilent-NMR-vnmrs600. Thermal gravimetric analyses (TGA) were performed under N_2 atmosphere with a heating rate of $10\text{ }^\circ\text{C}/\text{min}$ using TGA Q500 instrument. Powder X-ray diffraction (XRD) patterns were recorded on Rigaku D/MAX2550 Diffractometer using $\text{Cu K}\alpha$ radiation ($\lambda = 1.5406\text{ \AA}$), with a scan speed of $1^\circ/\text{min}$. The N_2 sorption-desorption and Brunauer-Emmett-Teller surface area measurements were carried out on a Micrometrics ASAP 2460 volumetric gas adsorption analyzer. Scanning electron microscopy (SEM) was performed on JSM-7500F. Transmission electron microscopy (TEM) was performed on a FEI Tecnai G2 S-Twin with a field emission gun operating at 200 kV. Images were acquired digitally on a Gantan multiple CCD camera. Energy dispersive spectroscopy (EDS) spectra were obtained using a JEOL JSM-6300 at 5 kV. X-ray photoelectron spectroscopy (XPS) measurements were performed on an ESCALAB 250 X-ray photoelectron spectroscopy, using $\text{Mg K}\alpha$ X-ray as the excitation source.

Synthetic Procedures

Synthesis of 1,3,5-triformylphloroglucinol (Tp)

1,3,5-triformylphloroglucinol (Tp) was synthesized according to a reported procedure.^[1] To hexamethylenetetramine (15.098 g, 108 mmol) and dried phloroglucinol (6.014 g, 49 mmol) under N_2 was added 90 mL trifluoroacetic acid. The solution was heated at $100\text{ }^\circ\text{C}$ for 2.5 h. Then 150 mL of 3 M HCl was added and the solution was heated at $100\text{ }^\circ\text{C}$ for 1 h. After cooling to room temperature, the solution was filtered through celite, extracted with CH_2Cl_2 $3\times 100\text{ mL}$, dried over magnesium sulfate, and filtered. The filtrate was concentrated using a rotary evaporator. The crude residue was purified by washing with hot ethanol to give pure Tp as a pink-white solid. Yield: 12 %.

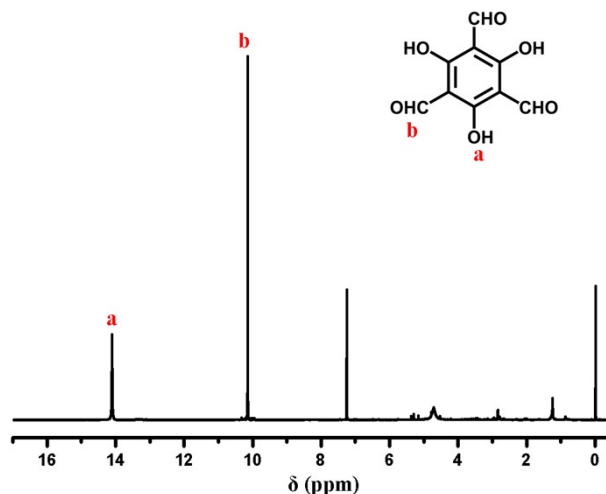
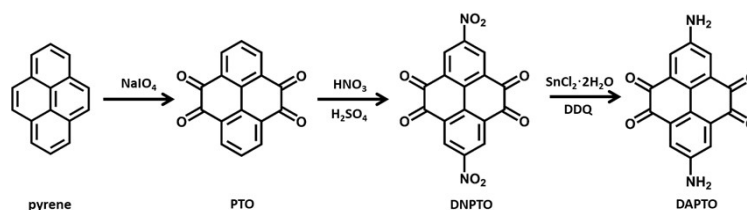


Figure S1. ^1H NMR spectra (400 MHz, CDCl_3) of Tp: δ 14.10 (s, 3H), 10.14 (s, 3H) ppm.

Synthesis of 2,7-Diaminopyrene-4,5,9,10-tetraone (DAPTO) [2]



Pyrene-4,5,9,10-tetraone (PTO). To a solution of pyrene (5 g, 25.4 mmol) in CH_2Cl_2 (100 mL) and acetonitrile (100 mL) was added NaIO_4 (44.5 g, 207.9 mmol), H_2O (125 mL), and $\text{RuCl}_3 \cdot x\text{H}_2\text{O}$ (0.64 g, 3.1 mmol). The suspension was heated at 40°C overnight. The organic solvents of the reaction mixture were removed under reduced pressure. A dark green cake was obtained by filtrating the residue and rinsing with 500 mL of H_2O , dried in air at 70°C , and subjected to column chromatography (CH_2Cl_2) to afford PTO as golden needles. Yield: 15 %.

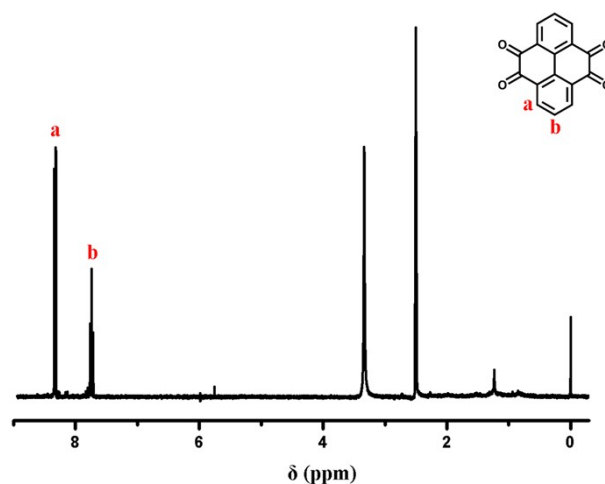


Figure S2. ^1H NMR spectra (400 MHz, $\text{DMSO-}d_6$) of PTO: δ 8.33 (d, 4H), 7.74 (t, 2H) ppm.

2,7-Dinitropyrene-4,5,9,10-tetraone (DNPTO). A mixture of fuming nitric acid (1.3 mL) and 98% sulfuric acid (1.3 mL) was added dropwise to PTO (524 mg, 2.0 mmol), and the resulted orange solution was heated at 85 °C. The same amount of the mixed acid was added to the flask for two more times at a 1-hour interval. After additional reaction for 1 h, the suspension was poured into 25 mL of H_2O , rinsed with another 100 mL of H_2O , and dried in vacuum to afford DNPTO as a bright yellow powder which was used without further purification. Yield: 83%.

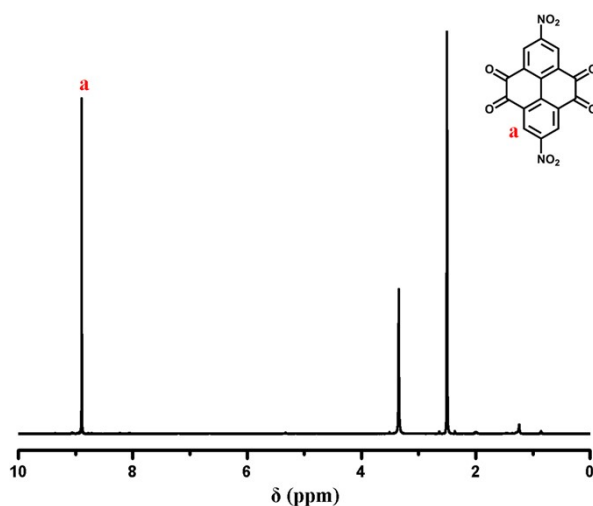


Figure S3. ^1H NMR spectra (400 MHz, $\text{DMSO-}d_6$) of DNPTO: δ 8.89 (s, 4H) ppm.

2,7-Diaminopyrene-4,5,9,10-tetraone (DAPTO). Acetic acid (2.0 mL) and concentrated hydrochloric acid (2.0 mL) were added to DNPTO (200 mg, 0.57 mmol) to form a yellow suspension, to which $\text{SnCl}_2 \cdot 2\text{H}_2\text{O}$ (1.02 g, 4.5 mmol) was slowly

added and the mixture was heated at 50 °C for 15 min. Gray solids were obtained by filtration and dried under vacuum. The gray solid (190 mg) and 2,3-dichloro-5,6-dicyano-1,4-benzoquinone (283 mg, 1.3 mmol) were then suspended in dry methanol (4.2 mL) under Ar and stirred at 35 °C for 15 h. The reaction mixture was diluted with ethylacetate (25 mL), and the dark purple precipitate was filtered, washed with ethylacetate, and dried under vacuum and used without further purification. Yield: 64%.

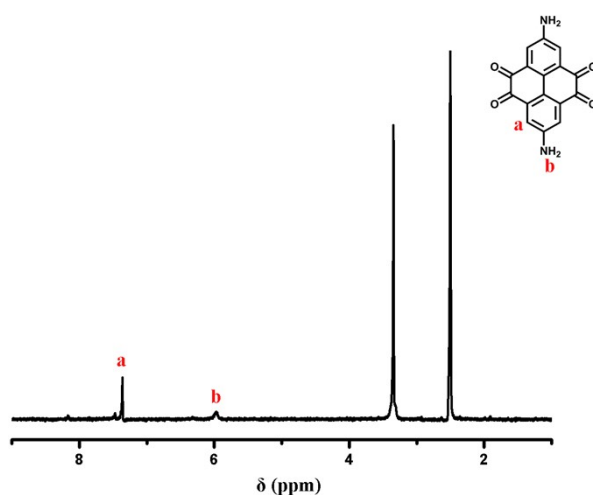


Figure S4. ^1H NMR spectra (400 MHz, $\text{DMSO-}d_6$) of DAPTO: δ 7.32 (s, 4H), 5.93 (s, 4H) ppm.

Synthesis of Tp-PTO-COF

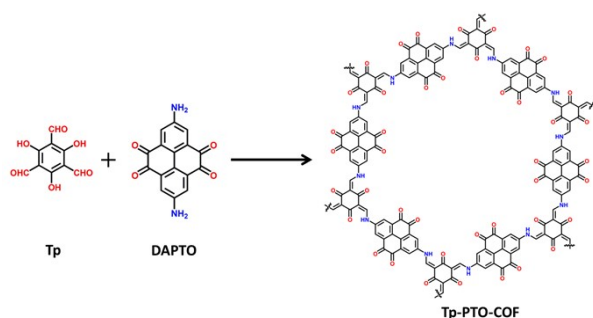


Figure S5. Synthesis route for Tp-PTO-COF.

A glass tube was charged with Tp (20 mg, 0.095 mmol) and DAPTO (41 mg, 0.142 mmol) in a mixed solution of dioxane (0.6 mL) and mesitylene (0.6 mL). The resulting suspension was sonicated, and then added 50 μL portion of 6 M acetic acid. After three freeze-pump-thaw cycles, the tube was vacuumed and flame-sealed. The ampoule was warmed to room temperature before heating to 120 °C for 5 d. The

resulting precipitates were collected by filtration and washed with DMF till filtrate became colorless. Further purification of the material was carried out by Soxhlet extraction in methanol and THF. Then the material was dried at 80 °C under vacuum for 12 hours to afford Tp-PTO-COF as a black powder. Elemental analysis for the calculated ($C_{66}H_{24}N_6O_{18}$): C: 66.67; H: 2.02; N: 7.07%. Found: C: 65.21; H: 2.55; N: 6.83%.

Synthesis of Tp-PTO-POF

The synthetic process was similar to Tp-PTO-COF, except for the constant stirring.

Characterization

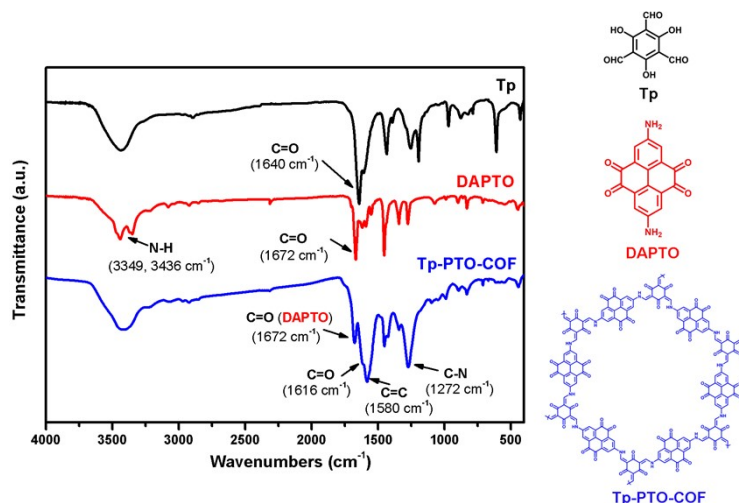


Figure S6. FT-IR spectra of Tp (black), DAPTO (red), and Tp-PTO-COF (blue).

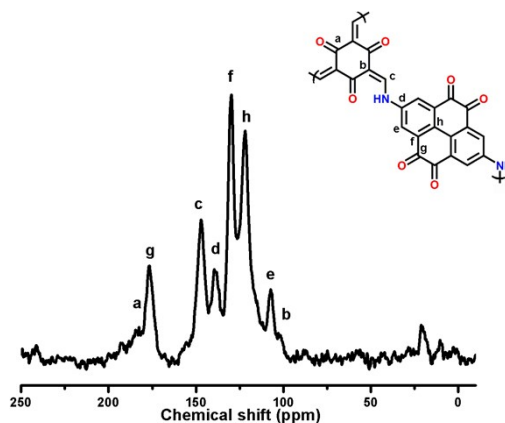


Figure S7. Solid-state ^{13}C CP/MAS NMR of Tp-PTO-COF.

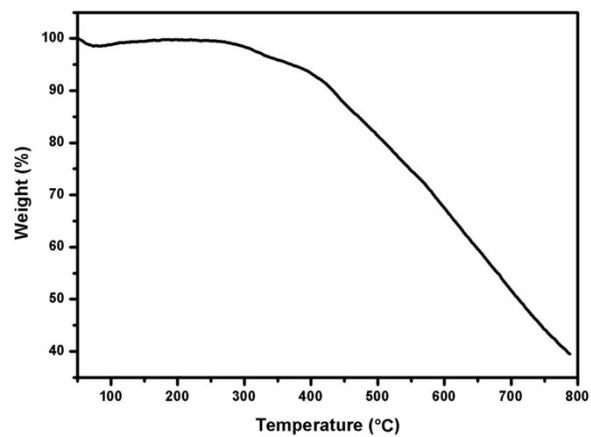


Figure S8. TGA curve of Tp-PTO-COF.

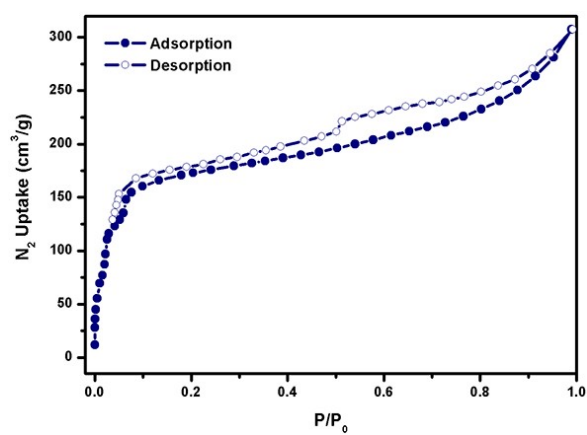


Figure S9. N₂ adsorption and desorption isotherms of Tp-PTO-COF.

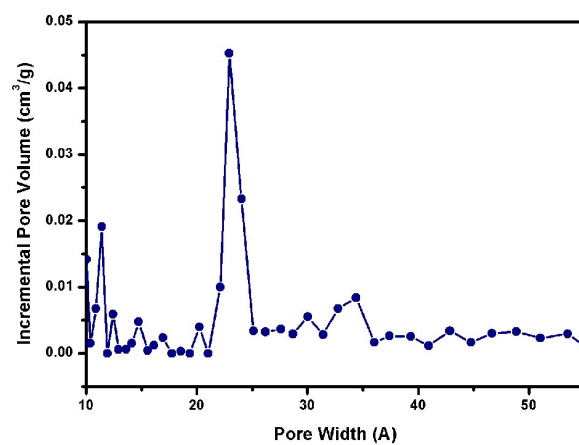


Figure S10. Pore size distribution of Tp-PTO-COF.

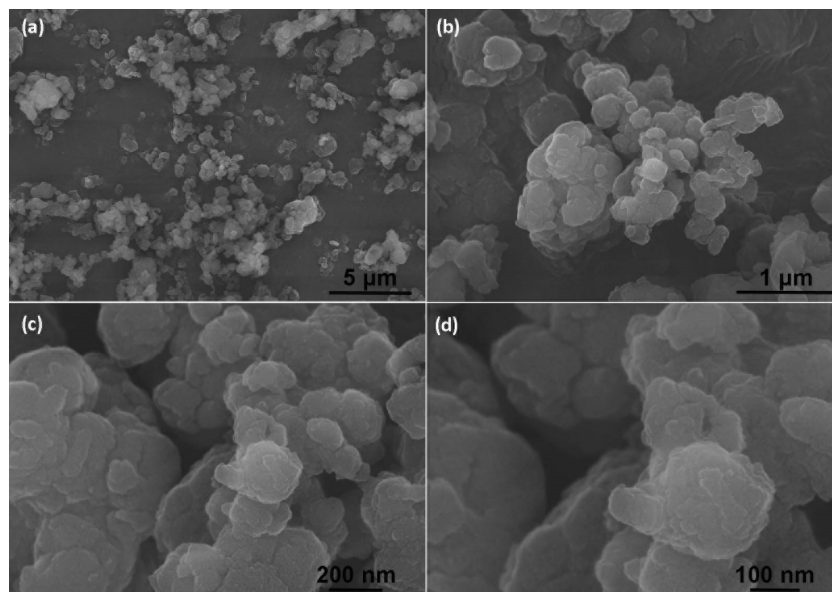


Figure S11. SEM images of Tp-PTO-COF.

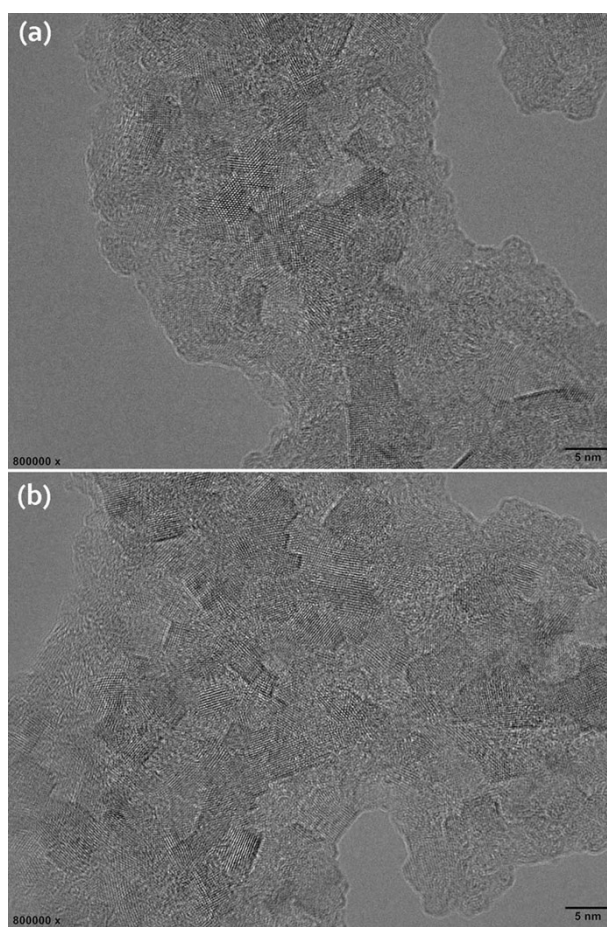


Figure S12. HRTEM images of Tp-PTO-COF.

Structure simulations and powder X-ray diffraction analyses

Structural modeling of Tp-PTO-COF was carried out in the Accelrys Materials Studio software package. At first, the powder indexing was proceeded in the Reflex module in DICVOL91 program. Then empty unit cells were built with the above unit cell parameters. Single layer models were generated by connecting monomer fragments and filled into the unit cells. Eclipsed AA and staggered AB stacking arrangements were constructed with the above unit cell parameters and the lattice models were geometry optimized using the Forcite module (Universal forcefield, Ewald summation method). The experimental PXRD patterns agreed well with the simulations from the eclipsed AA layer stacking models. Finally, Pawley refinements of the eclipsed AA stacking models against the experimental PXRD patterns were applied to define the lattice parameters, producing the refined PXRD profiles, R_{wp} and R_p values.

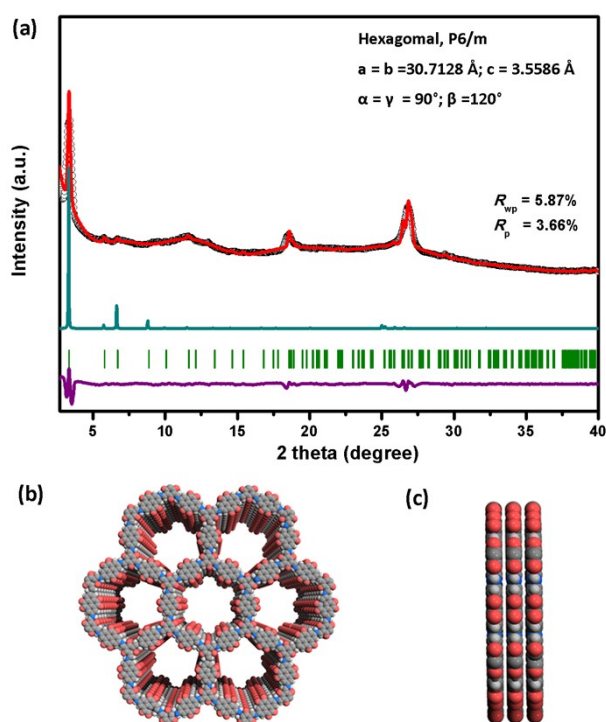


Figure S13. (a) A comparison between the experimental profiles (black dot), Pawley refined profiles (red line), simulated patterns for eclipsed (AA) stacking mode (cyan line), Bragg positions (green bar), and the refinement differences (violet line); (b, c) Top and side views of simulated eclipsed AA structure of Tp-PTO-COF.

Table S1. Fractional atomic coordinates for the eclipsed AA-stacking unit cell of Tp-PTO-COF.

Space group: $P6/m$

International tables number: 175

Cell setting: Hexagonal

$a = b = 30.7128 \text{ \AA}$; $c = 3.5586 \text{ \AA}$

$\alpha = \gamma = 90^\circ$; $\beta = 120^\circ$

Atom site label	Atom site type symbol	x	y	z	Atom site Uiso or equiv	Atom site adp type	Atom site occupancy
C1	C	-0.35732	0.27689	0.5	0.05	Uiso	1
C2	C	-0.30167	0.30988	0.5	0.05	Uiso	1
C3	C	-0.01581	0.40813	0.5	0.05	Uiso	1
C4	C	0.06033	0.49678	0.5	0.05	Uiso	1
C5	C	-0.13383	0.41846	0.5	0.05	Uiso	1
C6	C	-0.10136	0.3988	0.5	0.05	Uiso	1
N7	N	-0.18743	0.38385	0.5	0.05	Uiso	1
C8	C	-0.22595	0.39797	0.5	0.05	Uiso	1
H9	H	-0.11719	0.3583	0.5	0	Uiso	1
H10	H	-0.19751	0.34605	0.5	0	Uiso	1
H11	H	-0.21362	0.43763	0.5	0	Uiso	1
C12	C	0.03928	0.44165	0.5	0.05	Uiso	1
C13	C	-0.04888	0.43032	0.5	0.05	Uiso	1
C14	C	0.11277	0.52904	0.5	0.05	Uiso	1
H15	H	0.1362	0.51214	0.5	0	Uiso	1
C16	C	0.02792	0.51699	0.5	0.05	Uiso	1
O17	O	-0.57541	0.35695	0.5	0	Uiso	1
O18	O	-0.28968	0.434	0.5	0	Uiso	1
O19	O	-0.60311	0.03438	0.5	0	Uiso	1

Electrochemical measurement

Electrochemical measurements were performed using CR2016 coin type cells on a LAND CT2001A battery tester and Gamry Reference 3000 at room temperature between 0.4 and 1.5 V. The working electrode was prepared by mixing Tp-PTO-COF as active materials with conductive additive (Super P) and binder (PVDF) in a mass ratio of 60:35:5 in NMP. Then the slurry was coated on a carbon paper current collector and dried at 80 °C overnight in air. The cathode was cut into a round shape with a diameter of 12 mm, and the mass loading density of the active materials is about 0.6 mg cm⁻². The cells were thus fabricated from the cathode, a glass fiber membrane, a Zn foil anode and 2 M ZnSO₄ aqueous solution as electrolyte. Cyclic voltammetry (CV) measurements were performed on a CHI660E electrochemical workstation in the potential between 0.4 and 1.5 V vs. Zn²⁺/Zn at a scan rate from 0.5 to 3 mV s⁻¹. The electrochemical impedance spectroscopy (EIS) test was carried out on a CHI660E electrochemical workstation in the frequency range from 100 kHz to 10 mHz with an amplitude of 5 mV.

The dynamics of zinc ion was tested by galvanostatic intermittence titration technique (GITT) technique. The batteries were performed for 20 min galvanostatic pulse (charge or discharge) at a current density of 0.03 A g⁻¹. The Zn²⁺ ion diffusion diffusivity (D) was obtained *via* the following equation^[3-5]:

$$D = \frac{4l^2}{\pi\tau} \left(\frac{\Delta E_s}{\Delta E_t} \right)^2$$

where τ represents the constant current pulse time, l represents the thick of the cathode. ΔE_s is the change of steady-state voltage during a single-step GITT experiment, and ΔE_t stands for the total change of cell voltage during a constant current pulse τ of a single-step GITT experiment regardless of the IR-drop.

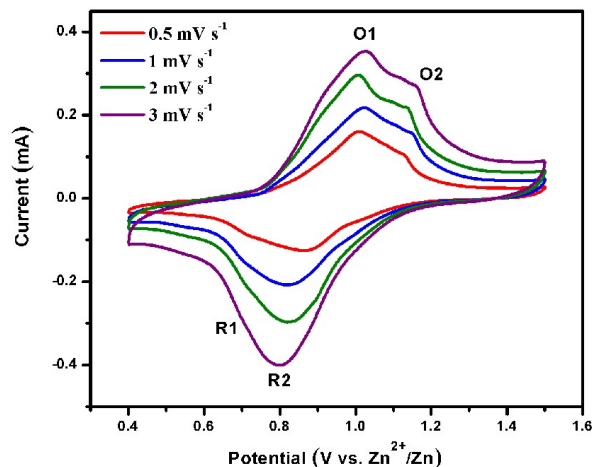


Figure S14. CV curves of Zn/Tp-PTO-COF battery at sweeping rates of 0.5, 1, 2, and 3 mV s^{-1} , respectively.

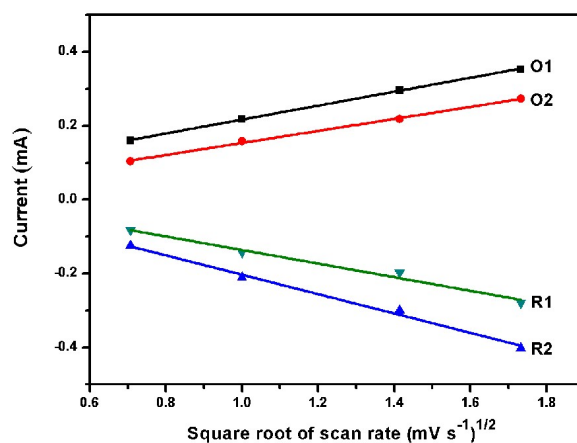


Figure S15. The linear relation of cathodic peak current vs. square root of scan rate for Tp-PTO-COF.

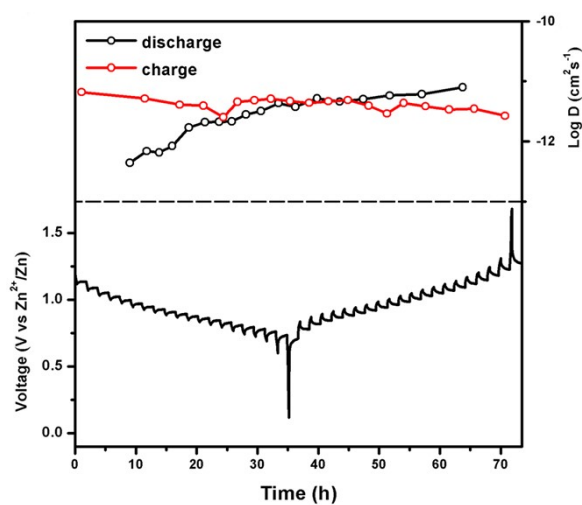


Figure S16. The GITT curves and calculated diffusion coefficients of Tp-PTO-COF during cycling under 0.03 A g^{-1} .

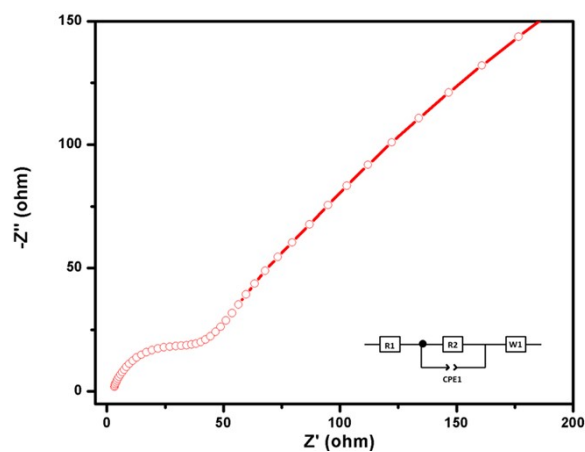


Figure S17. The EIS of Tp-PTO-COF. Inset is the equivalent circuit used for fitting the electrochemical impedance data.

Table S2. Fitted values of elements in the equivalent circuit for EIS data of Tp-PTO-COF.

	R_s (Ω)	R_{ct} (Ω)	CPE1-T	CPE1-P	W1-T	W1-P
Tp-PTO-COF	2.542	29.08	3.836×10^{-6}	0.8974	0.0174	0.506

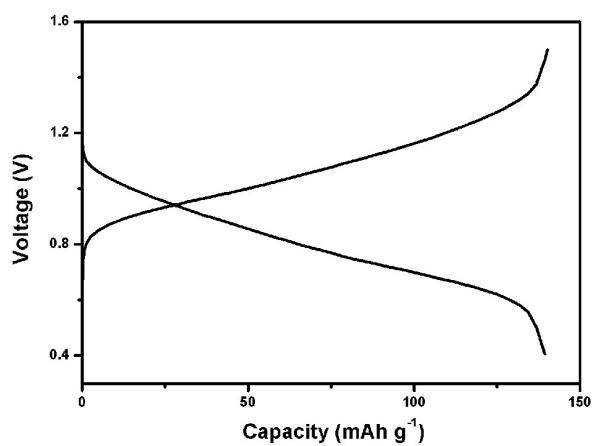


Figure S18. Galvanostatic charge-discharge curves of the aqueous Zn/Tp-PTO-COF battery at the current density of 10 A g⁻¹.

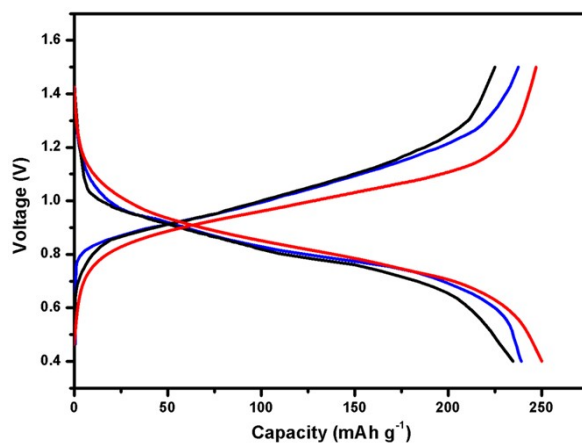


Figure S19. Galvanostatic charge-discharge curves of the aqueous Zn/Tp-PTO-COF batteries with different loading mass of Tp-PTO-COF at the current density of 1 A g^{-1} (red 0.6 mg cm^{-2} , blue 1.2 mg cm^{-2} and black 2.4 mg cm^{-2}).

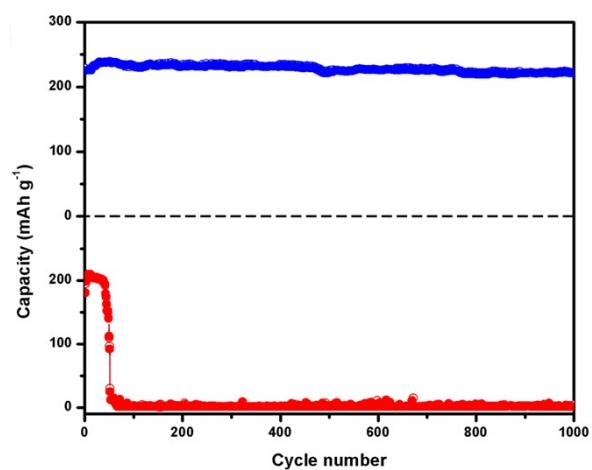


Figure S20. Cycle stability curves of the aqueous Zn/Tp-PTO-COF battery (blue) and Zn/Tp-PTO-POF battery (red) at the current density of 2 A g^{-1} .

Table S3. Comparative electrochemical performance of Tp-PTO-COF and other reported cathode materials for aqueous rechargeable ZIBs.

Material type	Electrode	Electrolyte	Voltage (V)	Current density (A g ⁻¹)	Capacity (mAh g ⁻¹)	Ref.
COFs	Tp-PTO-COF	2M ZnSO ₄	0.4-1.5	0.2	301.4	This work
				5	192.8	
	HqTP	3M ZnSO ₄	0.2-1.8	0.125	276	Chem. Sci. 2019, 10, 8889-8894
				3.75	85	
	PA-COF	1M ZnSO ₄	0.2-1.6	0.1	247	ACS Energy Lett. 2020, 5, 2256-2264
				5	93	
polymer	CLPy	30 M ZnCl ₂	0.5-1.8	0.2	150	Energy Environ. Sci. 2021,14, 462-472
				3	105	
	PDA	3.3 M ZnSO ₄	0.3-1.4	0.2	85	Chem. Commun., 2019, 55, 1647-1650
				5	43.2	
organic compounds	PTO	2M ZnSO ₄	0.36-1.46	0.1	300	Angew. Chem. Int. Ed. 2018, 57, 11737-11741
				5	162	
	tetrachloro-1,4-benzoquinone	1M Zn(OTf) ₂	0.8-1.4	0.217	118	Chem. Mater. 2018, 30, 3874-3881
	C4Q	3 M Zn(CF ₃ SO ₃) ₂	0.2-1.8	0.25	220	Sci. Adv. 2018, 4, 1761
				1	172	
	PQ-Δ	3 M Zn(CF ₃ SO ₃) ₂	0.25-1.6	0.03	225	J. Am. Chem. Soc. 2020, 142, 2541-2548
				0.15	210	
DTT	2M ZnSO ₄	0.3-1.4	0.2	175	Adv. Mater. 2020, 2000338	
			2	99		
inorganic compounds	PANI-intercalated MnO ₂	2 M ZnSO ₄ 0.1 M MnSO ₄	1.0-1.8	0.2	280	Nat. Commun. 2018, 9, 2906
				3	110	
	ZMO/C	3 M Zn(CF ₃ SO ₃) ₂	0.8-1.9	0.5	150	J. Am. Chem. Soc. 2016, 138, 12894-12901
				2	72	
	ZMO@Ti ₃ C ₂ Tx	1 M ZnSO ₄ 0.05 M MnSO ₄	0.8-1.8	0.2	150	Chem. Eng. J. 2020, 399, 125627
				4	84.5	
	HfO ₂ -coated ZVO	1 M ZnSO ₄	0.2-1.8	0.1	215	ACS Energy Lett. 2019, 4, 2776-2781
				3	88	
	Mg _{0.34} V ₂ O ₅ ·nH ₂ O nanobelts	3 M Zn(CF ₃ SO ₃) ₂	0.1-1.8	0.1	330	ACS Energy Lett. 2018, 3, 2602-2609
				5	81	
H ₂ V ₃ O ₈ nanowire	3 M Zn(CF ₃ SO ₃) ₂	0.2-1.6	0.5	279	Small 2017, 13, 1702551	
			5	155		

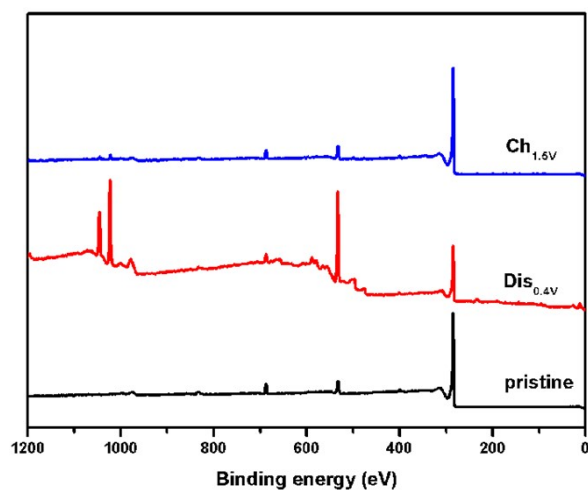


Figure S21. XPS spectra of Tp-PTO-COF electrode at pristine, fully discharged (0.4 V), and fully charged (1.5 V) states.

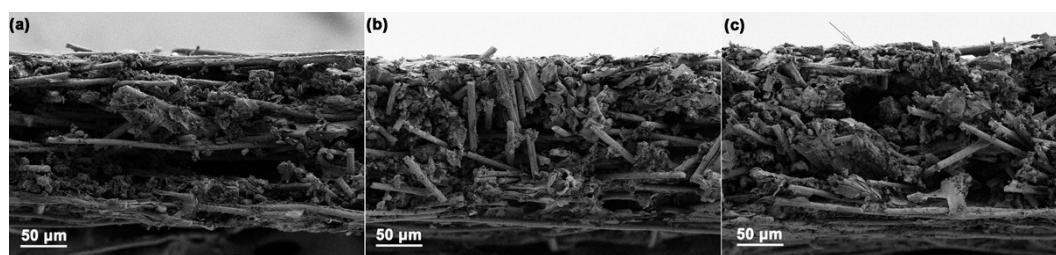


Figure S22. SEM images of Tp-PTO-COF cathode cross-sections during the charge-discharge process. (a) pristine, (b) fully discharged, and (c) fully recharged states after 50 cycles.

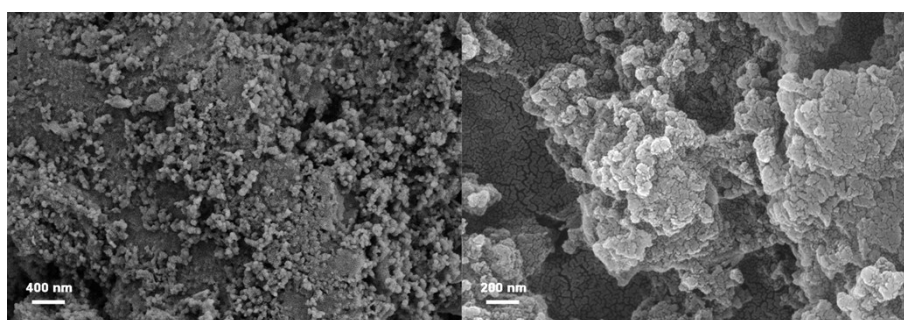


Figure S23. SEM images of Tp-PTO-COF cathode surface at pristine state.

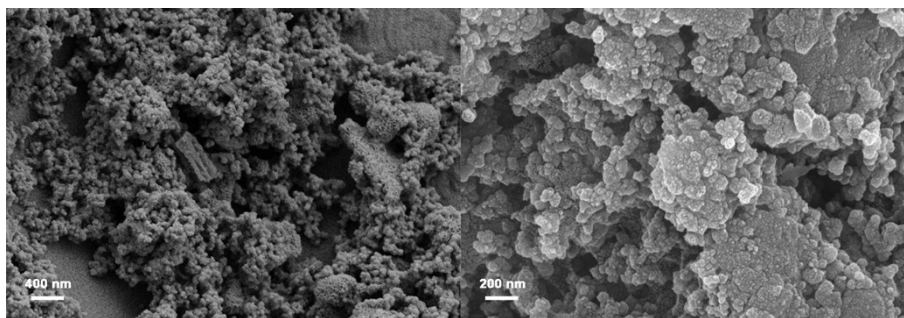


Figure S24. SEM images of Tp-PTO-COF cathode surface fully discharged state after 50 cycles.

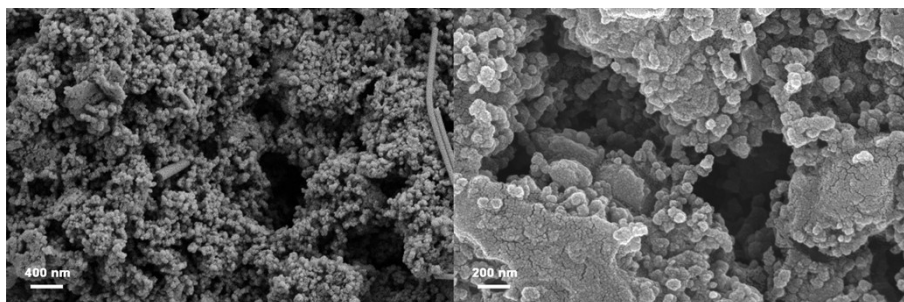


Figure S25. SEM images of Tp-PTO-COF cathode surface fully recharged states after 50 cycles.

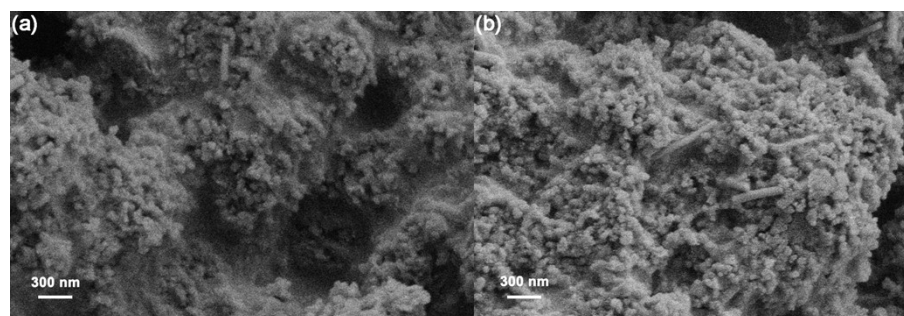


Figure S26. SEM images of Tp-PTO-COF cathode surface over 350 cycles. (a) fully discharged, and (b) fully recharged.

Theoretical calculation

All calculations were conducted using the Gaussian 16 software package.^[6] Geometry optimizations are performed at the B3LYP/6-31G* level of theory.^[7, 8] Calculations of the molecular electrostatic potential (MESP) were carried out using Multiwfn 3.8 programs.^[9]

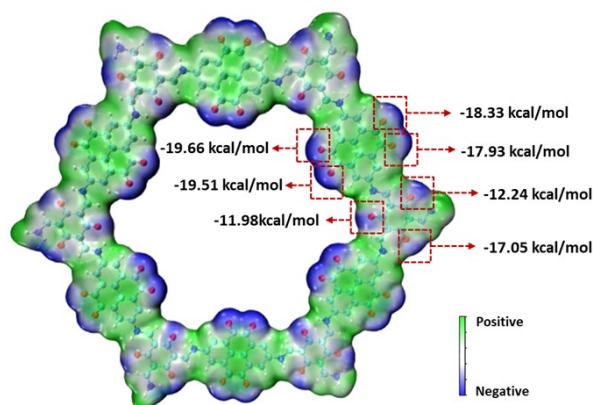


Figure S27. Electronegativity simulation of Tp-PTO-COF.

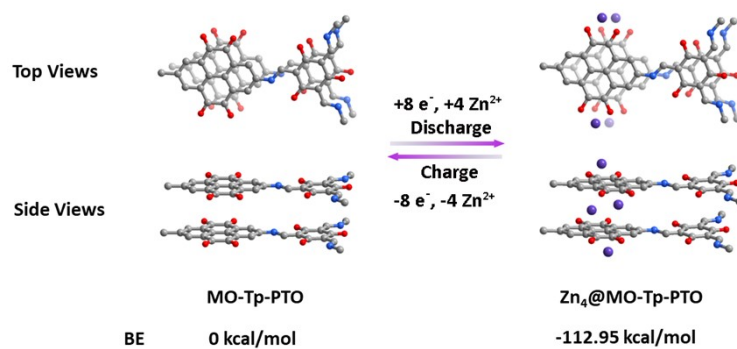


Figure S28. The DFT models of $Zn_4@MO-Tp-PTO$. Only adjacent carbonyl groups of PTO units as active sites for Zn uptaking.

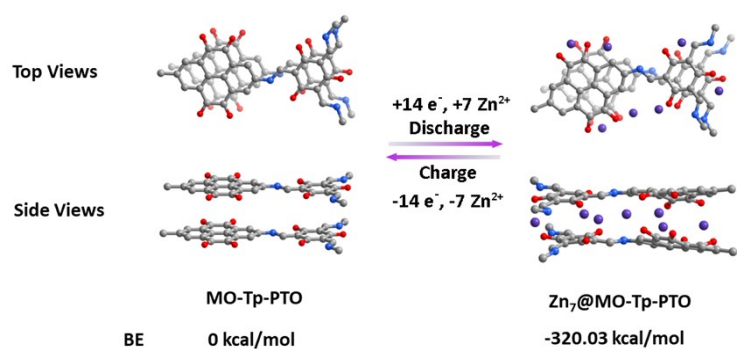


Figure S29. The DFT models of $Zn_7@MO-Tp-PTO$. In addition to carbonyl groups of PTO, two β -keto carbonyl groups bind with one Zn.

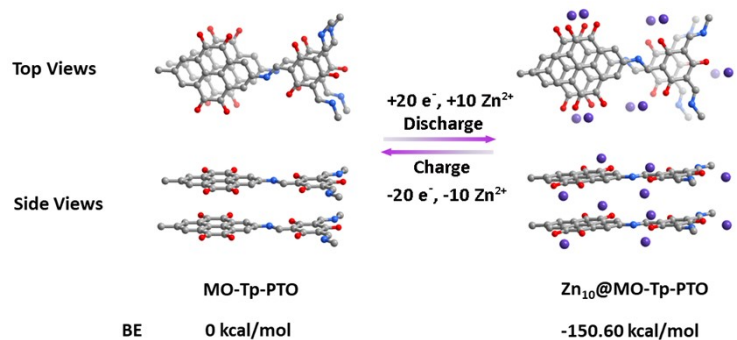


Figure S30. The DFT models of $Zn_{10}@MO-Tp-PTO$. In addition to carbonyl groups of PTO, each β -keto carbonyl group binds with one Zn.

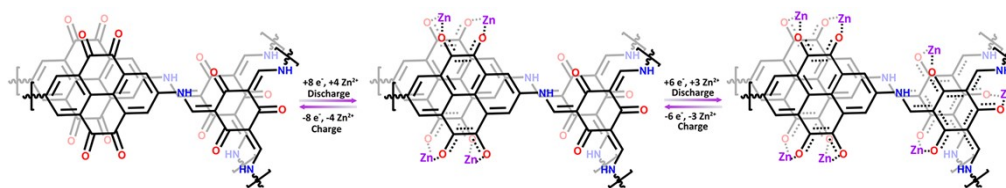


Figure S31. The possible mechanism of the interaction of Tp-PTO-COF with Zn^{2+} ions during the charge-discharge process in electrochemical reaction.

Table S4. Sum of electronic and zero-point energies and the binding energies (BE) calculated at the B3LYP/6-31G* level.

	MO-Tp-PTO	Zn	$\text{Zn}_4@$ MO-Tp-PTO	$\text{Zn}_7@$ MO-Tp-PTO	$\text{Zn}_{10}@$ MO-Tp-PTO
electronic and zero-point energies (hartree)	-3537.74	-1779.09	-10654.28	-15991.88	-21328.88
BE (hartree)			-0.18	-0.51	-0.24
BE (kcal/mol)			-112.95	-320.03	-150.60

$$\text{BE} = E(\text{Zn}_x@ \text{MO-Tp-PTO}) - E(\text{MO-Tp-PTO}) - x \cdot E(\text{Zn})^{[10,11]}$$

The theoretical capacity of Tp-PTO-COF is calculated from the following Equation:

$$C_t = \frac{\text{No. of electrons} \times 96485}{3600 \times \text{Molecular weight}} \times 1000$$

The molecular weight of Tp-PTO-COF is 1188 g·mol⁻¹, and there are 18 carbonyl groups served as active sites in each unit cell. Based on DFT model Zn₇@MO-Tp-PTO, there are 18 Zn²⁺ ions coordinating with the adjacent layers of Tp-PTO-COF unit cells, and the theoretical capacity is evaluated as 406 mA h g⁻¹.

The experimentally obtained discharge capacity = 301.4 mA h g⁻¹.

The efficiency of specific capacity = 74.23%.

References

- [1] Cong, J. H.; Sauer, M.; Patrick, B. O.; MacLachlan, M. J. Highly stable keto-enamine salicylideneanilines, *Org. Lett.*, **2003**, *5*, 3823-3862.
- [2] Liang, Y.; Jing, Y.; Gheyhani, S.; Lee, K.-Y.; Liu, P.; Facchetti, A.; Yao, Y. Universal quinone electrodes for long cycle life aqueous rechargeable batteries. *Nat. Mater.*, **2017**, *16*, 841-848.
- [3] Tang, W.; Lan, B.; Tang, C.; An, Q.; Chen, L.; Zhang, W.; Zuo, C.; Dong, S.; Luo, P. Urchin-like spinel MgV_2O_4 as a cathode material for aqueous zinc ion batteries, *ACS Sustainable Chem. Eng.*, **2020**, *8*, 3681-3688.
- [4] Ming, F.; Liang, H.; Lie, Y.; Kandambeth, S.; Eddaoudi, M.; Alshareef, H. N. Layered $\text{Mg}_x\text{V}_2\text{O}_5 \cdot n\text{H}_2\text{O}$ as cathode material for high-performance aqueous zinc ion batteries, *ACS Energy Lett.*, **2018**, *3*, 2602-2609.
- [5] He, P.; Quan, Y.; Xu, X.; Yan, M.; Yang, W.; An, Q.; He, L.; Mai, L. High-performance aqueous zinc-ion battery based on layered $\text{H}_2\text{V}_3\text{O}_8$ nanowire cathode, *Small* **2017**, *13*, 1702551.
- [6] Frisch, M. J.; Trucks, G. W.; Schlegel, H. B.; Scuseria, G. E.; Robb, M. A.; Cheeseman, J. R.; Scalmani, G.; Barone, V.; Petersson, G. A.; Nakatsuji, H.; Li, X.; Caricato, M.; Marenich, A. V.; Bloino, J.; Janesko, B. G.; Gomperts, R.; Mennucci, B.; Hratchian, H. P.; Ortiz, J. V.; Izmaylov, A. F.; Sonnenberg, J. L.; Williams-Young, D.; Ding, F.; Lipparini, F.; Egidi, F.; Goings, J.; Peng, B.; Petrone, A.; Henderson, T.; Ranasinghe, D.; Zakrzewski, V. G.; Gao, J.; Rega, N.; Zheng, G.; Liang, W.; Hada, M.; Ehara, M.; Toyota, K.; Fukuda, R.; Hasegawa, J.; Ishida, M.; Nakajima, T.; Honda, Y.; Kitao, O.; Nakai, H.; Vreven, T.; Throssell, K.; Montgomery, J. A., Jr.; Peralta, J. E.; Ogliaro, F.; Bearpark, M. J.; Heyd, J. J.; Brothers, E. N.; Kudin, K. N.; Staroverov, V. N.; Keith, T. A.; Kobayashi, R.; Normand, J.; Raghavachari, K.; Rendell, A. P.; Burant, J. C.; Iyengar, S. S.; Tomasi, J.; Cossi, M.; Millam, J. M.; Klene, M.; Adamo, C.; Cammi, R.; Ochterski, J. W.; Martin, R. L.; Morokuma, K.; Farkas, O.; Foresman, J. B.; Fox, D. J.; Gaussian 16, Gaussian, Inc., Wallingford CT, USA, **2016**.

- [7] Stephens, P. J.; Devlin, F. J.; Chabalowski, C. F.; Frisch, M. J. Ab initio calculation of vibrational absorption and circular dichroism spectra using density functional force fields. *J. Phys. Chem.*, **1994**, *98*, 11623-11627.
- [8] Petersson, G. A.; Bennett, A.; Tensfeldt, T. G.; Al-Laham, M. A.; Shirley, W. A.; Mantzaris, J. Complete Basis Set Model Chemistry. I. The total energies of closed-shell atoms and hydrides of the first-row elements. *J. Chem. Phys.*, **1988**, *89*, 2193.
- [9] Tian, L.; Feiwu C. Multiwfn: a multifunctional wavefunction analyzer, *J. Comput. Chem.*, **2012**, *33*, 580-592.
- [10] Miao, L.; Liu, L.; Shang, Z.; Li, Y.; Lu, Y.; Cheng, F.; Chen, J. The structure-electrochemical property relationship of quinone electrodes for lithium-ion batteries. *Phys. Chem. Chem. Phys.*, **2018**, *20*, 13478.
- [11] Peng, C.; Ning, G.-H.; Su, J.; Zhong, G.; Tang, W.; Tian, B.; Su, C.; Yu, D.; Zu, L.; Yang, J.; Ng, M.-F.; Hu, Y.-S.; Yang, Y.; Armand, M.; Loh, K. P. Reversible multi-electron redox chemistry of π -conjugated N-containing heteroaromatic molecule-based organic cathodes. *Nat. Energy.*, **2017**, *2*, 17074.